Final Report for Full-Scale Load Monitoring of Rubble Mound Breakwaters

description of work completed by Aalborg University

Burcharth, Hans F.; Frigaard, Peter; Helm-Petersen, Jacob; Schlütter, Flemming; Andersen, Henning

Publication date:
1995

Document Version
Accepted author manuscript, peer reviewed version

FINAL REPORT FOR FULL-SCALE LOAD MONITORING OF RUBBLE MOUND BREAKWATERS.

Contract No.: MAS2-CT92-0023

Description of work completed by Aalborg University.

Prof. Dr. techn.: H. F. Burcharth
Ass. Prof.: Peter Frigaard
Ph.D. Student: Jacob Helm-Petersen
Ph.D. Student: Flemming Schlütter
Assistant researcher: Henning Andersen

Contents:

I.1.1 Introduction

As associated partner, Aalborg University (AU) has participated in different aspects of "the Zeebrugge project". At an early stage AU has developed and tested an algorithm aiming at deducing incident waves at the prototype breakwater by reflection analysis. Secondly AU, has been engaged with the development of a numerical model able to predict the hydraulic response of the Zeebrugge breakwater. Finally, AU has carried out an extensive number of small-scale model tests (1:65) with the Zeebrugge breakwater with the aim of investigating scale-effects.

The paragraphs I.1.2 till I.2.2 and II.C.1, II.D.2 and II.D.3.2 render concisely the work carried out by AU and some of the proceeding Analyses of data. For more detailed and elaborate descriptions of the work done the reader is advised to confer with earlier published full progress reports or to contact Aalborg University directly.

I.1.2 Reflection analysis

The aim is to apply an algorithm which can calculate incident waves at the prototype breakwater in time domain given an assumption of a known reflection coefficient. Furthermore, the method requires that a time series is recorded at a distance to the breakwater.

The sensitivity of the method was evaluated concluding that if a reasonable reflection coefficient can be estimated, the proposed method yields a better estimate of the incident elevation signal, than if the reflection was ignored.

At a later point, the implementation of the method into the MAST-software was tested and a few proposals were made as corrections to the implementation.

I.1.3 Numerical modelling

A numerical model has been developed at AU. The aim is to provide insight into the physics concerning internal flow in porous structures as well as making it possible to conduct computations for comparison with prototype measurements and model tests.

A mathematical flow model for successive numerical implementation has to cover the complex phenomena evolving, when waves intercept a porous structure such as the Zeebrugge breakwater, i.e. up-rush, down-rush, infiltration, seepage and oscillations of the free and phreatic surface. Also material related parameters such as friction and porosity have to be considered. With this point of view the one-dimensional model FloX has been applied.

In order to establish a numerical model simulating external and internal flow processes, a set of hydraulic equations is needed. Within the permeable structure, the internal flow resistance is modelled by the extended Forchheimer equation. The one dimensional description is derived by vertical integration of the Navier-Stokes equations and the equation of continuity. For detailed description of the model please refer to the 1994 full progress report.

The model is a coupled model connecting the hydraulic model outside the porous structure with the porous flow through the face of the structure modelling a disconnected free surface and intrinsic water surface. Equations are solved by finite

differences using the dissipative Lax-Wendroff scheme as solution scheme.

Initially, the model was restricted to handling of homogeneous structures with the possibility of introducing an impermeable core. This model was verified against physical model tests conducted at Aalborg Hydraulics Laboratory. The model shows good performance considering the hydraulic response outside the breakwater where run-up and run-down levels are predicted with good agreement to the physical tests.

The porous flow does show correct characteristics but quantification of pressure amplitudes and setup levels have a deviant behaviour compared with prototype values. This problem has been attempted solved by looking into the connection between the free surface and the phreatic surface as clearly the pressure gradients are not modelled correctly at this point. Changing the gradient at the "shoreline" does make it possible to control the out/inflow in the breakwater more sensibly but does not help the modelling of the pressure amplitudes. This is a result of the one dimensional approach where the amplitudes inside the breakwater is too affected by the amplitudes outside the breakwater, i.e. run-up and run-down levels. It can therefore be concluded that the above mentioned problem is inextricably bound up with the complete structure of the numerical model.

It is possible to conclude that the chosen one dimensional formulation is not geared to simulate the highly complex flow inside the breakwater, a *fait accompli* which was not known beforehand. Still the model is applicable for some purposes. Some work has been done on implementing multiple layers within the model but this work has been abandoned as it was recognized that there was too little to gain. Finally, it must be concluded that a multidimensional model is needed for an adequately precise quantification of the internal hydraulic response of the Zeebrugge breakwater.

I.1.4 Physical model tests 1:65

AU has been involved with the execution of extensive physical model testing with the Zeebrugge breakwater. Conducting tests at a third scale 1:65 besides 1:20 and 1:30 makes it possible along with the prototype measurements to evaluate scale effects. In order to do this it is imperative to test models which are alike except for the scale and furthermore, to carry out identical test programmes. At the point in time when AU was to start testing, two different test strategies had already been applied at UCC and HRLB respectively. Where UCC had constructed a model with distorted scaling of the core material, HRLB had applied strict Froude scaling. Therefore, it was decided at AU to perform tests with both types of models

and furthermore, conduct tests on a third model with a third scaling of the core material thus permitting an evaluation of how to scale the core material in order to achieve a hydraulic response within the breakwater complying with the behaviour of the prototype.

The following five paragraphs describes the model setup. Where nothing else is stated, geometries and soforth is valid for all three models as the only difference is the applied core material.

I.1.4.1 Model setup

AU has both different flumes and basins available. It was decided to perform the tests in a shallow water bassin. Besides of the availability at that point in time, the decision was made in order to avoid using efforts on applying active wave absorption. Also it can be expected that larger setup occurs in the flume and long periodic waves are more predominant.

Model and wave generator was placed in the bassin with weakly reflecting rubble slopes at the edges. This placement is illustrated on figure 1.

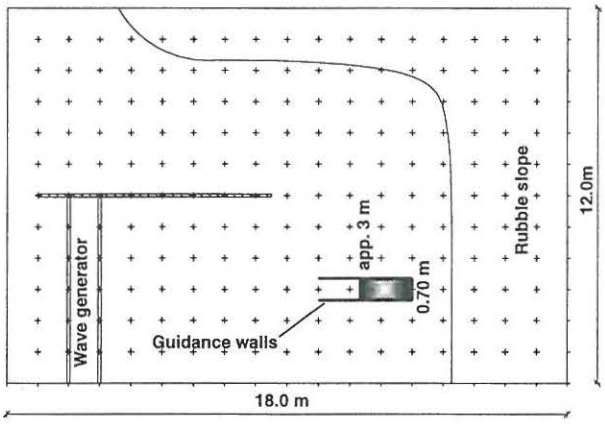

Figure 1: *Placement of model in wave bassin.*

I.1.4.2 Model description

The objective was to conduct small-scale tests and as Flanders Hydraulics Laboratory (HRLB) was able to provide small-scale antifer blocks, these were used. One hundred blocks were weighted and the density determined resulting in the data shown in table 1.

Small-scale antifer cubes	
Mean density: $\rho_m = 2341.57\frac{kg}{m^3}$	
Weights	Nominal diameter
$W_{15} = 85.34gr$	$D_{15} = 3.32cm$
$W_{50} = 86.86gr$	$D_{50} = 3.34cm$
$W_{85} = 88.33gr$	$D_{85} = 3.35cm$
$W_{mean} = 86.02gr$	$D_{\frac{15}{85}} = 0.9886$

Table 1: *Model antifer cubes.*

Applying the formula, taking into account the use of fresh water in the laboratory facility, the scale of the model antifers can be deduced as

$$\lambda = \left(\frac{W_n}{W_m\ 1.03}\right)^{\frac{1}{3}} \tag{1}$$

where W_n is the weight of the antifers in prototype and W_m in model. This results in a scale of $\lambda = 65.377$.

Characteristics of the geometry and materials in prototype has been reported in previous full-progress reports. These informations were used to determine scaled values for the first AU model which was strictly Froude scaled. The material characteristics for this model is seen in table 2.

Material	D_{15}	D_{50}	D_{85}	W_{50}	ρ
Core	0.18 cm	0.40 cm	0.59 cm	0.12 gr	$2.65t/m^3$
Filter	1.43 cm	1.64 cm	1.74 cm	8.18 gr	do.
Toe	1.66 cm	1.80 cm	1.95 cm	10.8 gr	do.
Armour	-	3.76 cm	-	86.9 gr	$2.34t/m^3$
Seagravel	-	0.19 mm	0.53 mm	0.013 gr	$2.65t/m^3$
Seasand	-	0.0031 mm	-	-	do.
Willow 1	-	-	-	$37gr/dm^3$	do.
Willow 2	-	-	-	$111gr/dm^3$	do.

Table 2: *Froude scaled materials.*

The model was constructed according to Froude scaling without modelling the

seabed topography in front of the breakwater. Page 10 holds a plot of the breakwater. Backfilling and seabed were closed of from the rest of the model by the use of plastic sheets as the seasand could not be scaled to the required very small grain size (0.0031 mm). As willow mattresses a geotextile was applied performing the protective task of the willow mattresses in prototype. The core of the model was infiltrated with sand to the level recorded in prototype.

Two additional models were constructed at AU and subsequently tested. The second with the core material scaled as $\lambda = 20$ and the third using the scale $\lambda = 40$. The distorted scaling of the second model was determined using the method of Le Mehaute as done at UCC (see full progress report 1994). This results in a scaling of the core material of $\lambda = 16$ till $\lambda = 24$ depending on the incident wave heights. A scale of 1:20 was applied due to the availability of such a material.

Third scaling of the core was decided on the basis of the hydraulic response of the latter two models, with the aim of matching the prototype.

I.1.4.3 Instrumentation

Instrumentation consisted of three wave gauges a run-up gauge and twelve pressure sensors. Wave gauges was placed relative to the breakwater axis as shown on figure 2.

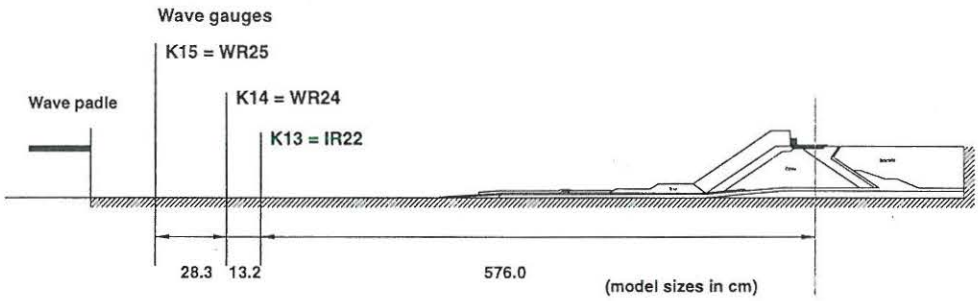

Figure 2: *Location of wave gauges relative to breakwater axis.*

The run-up gauge was, like the wave gauges, a resistance type gauge and this was placed on the face of the breakwater.

Twelve rigid tubes with a perforated cross-beam was placed inside the breakwater core according to the locations of pressure sensors in the prototype as they were 1/1-95. Outside the model, the pressure sensors were fitted to the end of the tubes

carefully ensuring that no trapped air was contained in the system. The pressure measurement system has earlier been used at AU and its usability verified. In figure 2 an illustration of the system is seen.

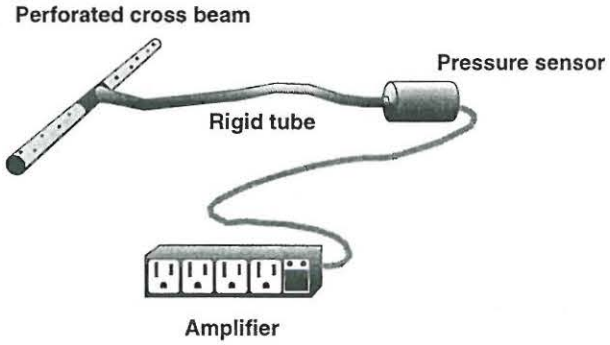

Figure 3: *Illustation of pressure measurement system.*

I.1.4.4 Conduction of tests

Tests with irregular waves were carried out using a Pierson-Moskowitz spectrum and filtering of white noise was used as generation method.

Sensor signals were sampled in all tests using a sampling frequency of $f = 10hz$. This results in signal descriptions with clearly sufficient resolution.

Test results are available as one file pr. test or one file pr. channel for each test. The structure of the database enables the use of the MAST-software developed by Elis. Scaling in this system is though limited applicable sample frequencies in prototype being restricted to integers. Specialized software for the analysis of the model test data from AU has been developed.

The conducted tests programme consists of a number of tests with both regular and irregular waves. Table 3 shows the test programme applied for all three sets of model tests at AU where values are expressed in prototype units.

As seen tests have been carried out at four different water levels and it should therefore be noticed that some sensors will be out of the water during a number of the tests. The duration of each test lasted 9000 data points corresponding to fifteen minutes in model scale.

I.2.1 Test programme

Please refer to paragraph I.1.4.4.

I.2.2 Available results

Results are available from three small-scale models constructed at AU. Data have been collected during an extensive test programme resulting in more than thirteen million numbers. These results of course cannot be rendered here. Due to the vast amount of data, AU has used the analysis strategy not analyzing all time series, but selecting relevant data for specific desired analyses. Some results of this approach can be seen in paragraphs II.C.1 and II.D.2.

Irregular waves

$H_s[m]$	$Z = +4.62m$	$Z = +2.47m$	$Z = +5.92m$	$Z = +0.32m$
1.0		X		X
1.5	X		X	
2.0	X	X	X	X
2.5	X			
3.0	X	X	X	X
3.5	X			
4.0	X	X	X	
4.5	X			
5.0	X			

Regular waves

$H[m]$	$T = 5.0s$	$T = 6.0s$	$T = 7.0s$	$T = 8.0s$	$T = 9.0s$
3.0	X	X	X	X	X
4.0	X	X	X	X	X

Table 3: *Test programme.*

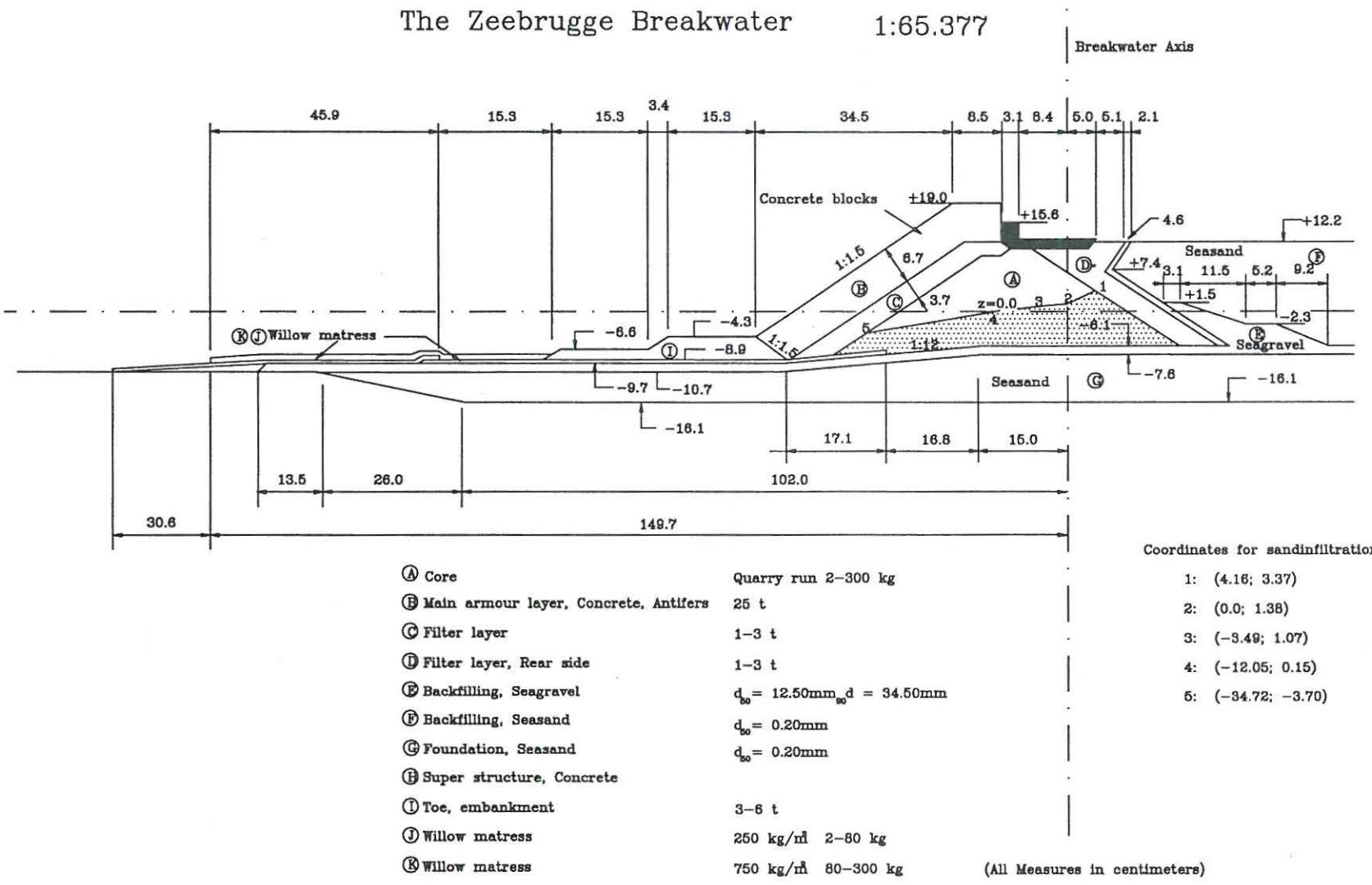

Figure 4: *Plot of model geometry.*

II.C.1 Internal set-up

In this Section the internal set-up in the Zeebrugge Breakwater is considered. Only results obtained from irregular waves are shown. For the model tests a Pierson-Moskowitz spectrum has been applied. The water level corresponds to $z = +4.62$ m. First, a simple theoretical formulation of internal set-up is presented (Barends, 1988), and secondly, the measured set-up is shown both as a function of the position in the core and the incident wave height. This analysis is applied to both prototype measurements and model scale tests. Finally, a comparison between the measured set-up and the theoretical set-up is given.

II.C.1.1 Introduction

When considering a conventional breakwater under wave attack, an internal set-up is likely to occur. This internal set-up can be explained by considering the length and cross-section of a flow tube during inflow and outflow. During inflow, the cross-section is relatively large and the penetration length is relatively short. Outflow takes place in the lower part of the breakwater when the phreatic surface is low i.e., the flow lines are long. In order to obtain an outflow which equals the inflow, the outflow velocity must be higher than the inflow velocity, which requires a high pressure gradient. Eventually, this leads to an internal set-up, because this set-up increases the pressure gradient during outflow and decreases the inflow.

II.C.1.2 Theoretical formulation of set-up

The maximum average internal set-up can be estimated by the simple theoretical expression presented by Barends (1988):

$$\frac{s}{D} = \sqrt{1 + \xi F} - 1 \tag{2}$$

where

$$\xi = \frac{0.1cH^2}{n\lambda D tan\alpha} \quad ; \quad \lambda = 0.5\sqrt{\frac{DKt}{n}} \tag{3}$$

where

s : maximum average set-up [m]
D: depth at toe of slope [m]
c : constant depending on effects of air entrainment and run-up (c>1)
H: wave height at slope [m]
n : effective porosity [-]

λ : penetration length of the cyclic water level into the porous structure [m]
α : slope angle [°]
K: permeability [m/s]
t : period of cyclic loading [S]
F: function depending on the rear side of the breakwater (open or lee-side) [-]

Normally, the magnitude of the internal set-up is within 10-20 % of the water depth at the toe of the breakwater (D) (Barends, 1988), or within 10-20 % of the incident wave height (Bürger et al. ,1988).

II.C.1.3 Internal set-up in the Zeebrugge Breakwater

The internal set-up in the Zeebrugge Breakwater is determined from both prototype measurements and model scale tests. The set-up is determined as the mean of the pore pressure records within the core of the breakwater (all pressures are equal to zero at SWL).

II.C.1.3.1 Set-up as a function of distance from filter-core interface

In Figures 5-11 the set-up for both prototype and model tests are shown as a function of the horizontal distance from the interface between the filter and the core. Only the pressure transducers located at elevation $z = 2.30$ m have been applied.

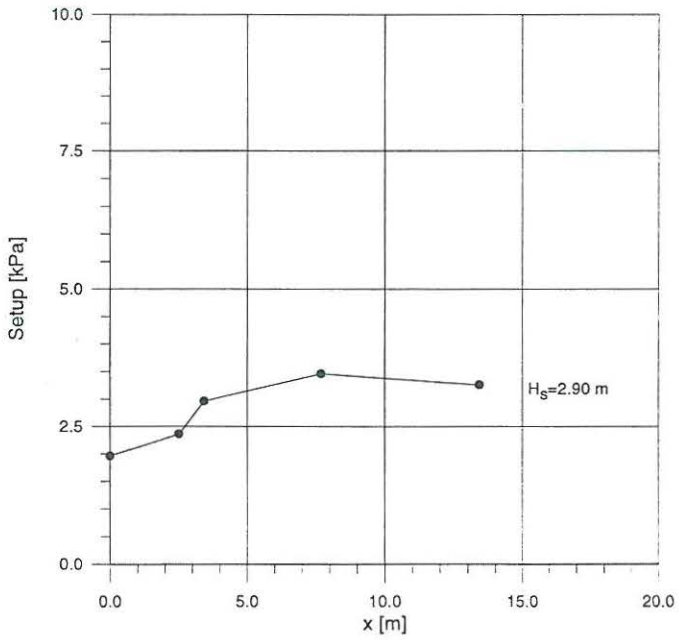

Figure 5: *Set-up in prototype.*

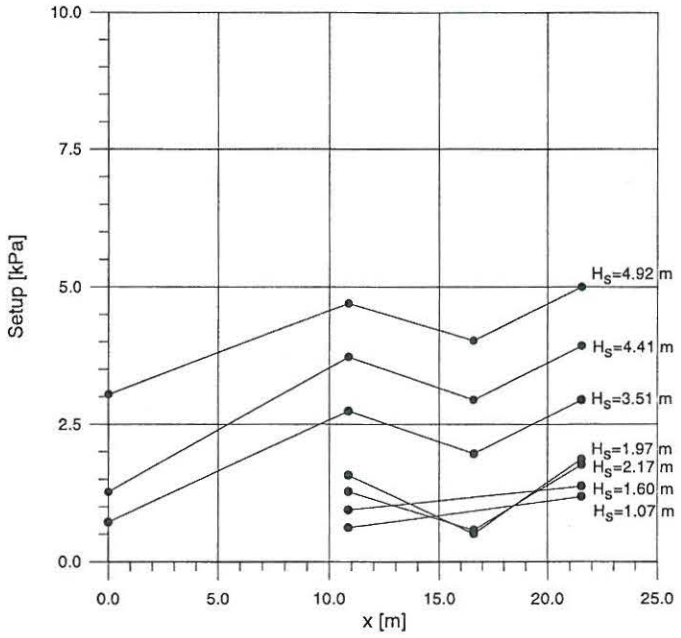

Figure 6: *Set-up in 1:20 model (without sandfilled core) (Prototype units).*

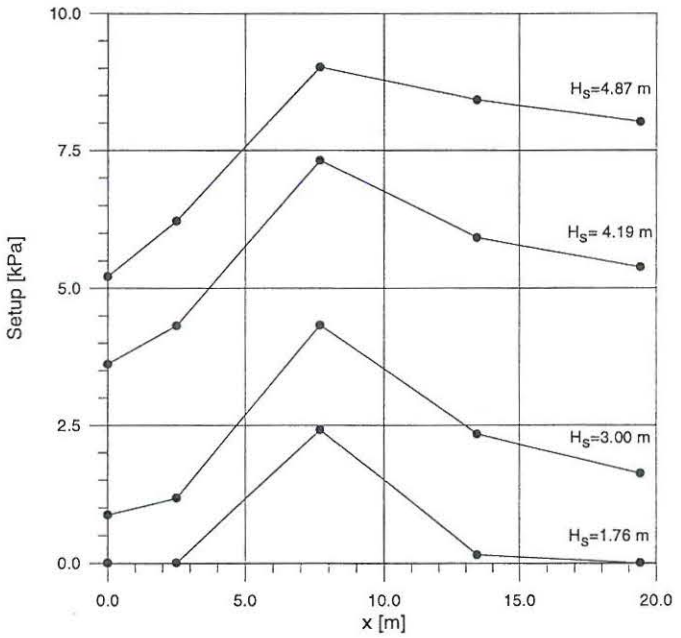

Figure 7: *Set-up in 1:20 model (Prototype units).*

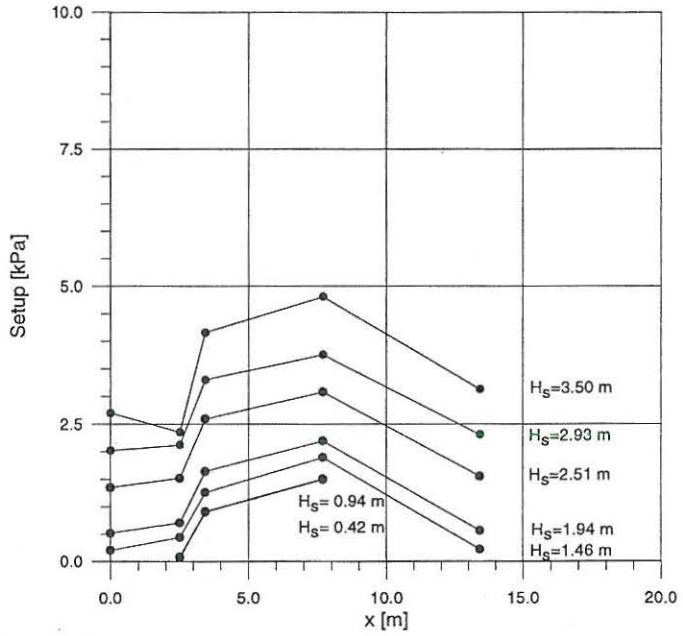

Figure 8: *Set-up in 1:30 model (distorted core 1:10) (Prototype units).*

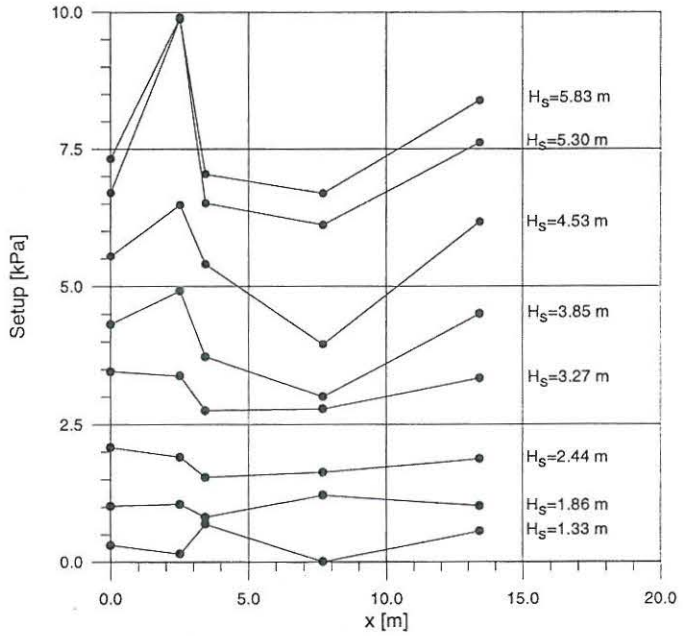

Figure 9: *Set-up in 1:65 model (Prototype units).*

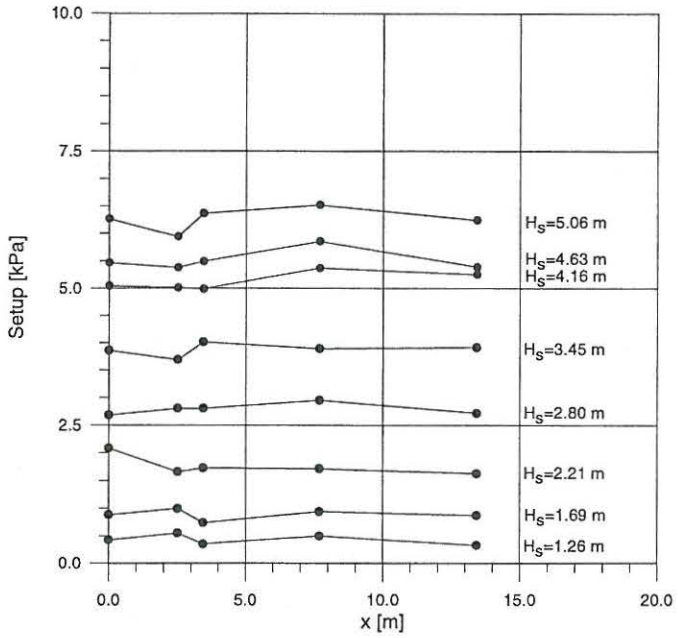

Figure 10: *Set-up in 1:65 model (distorted core 1:40) (Prototype units).*

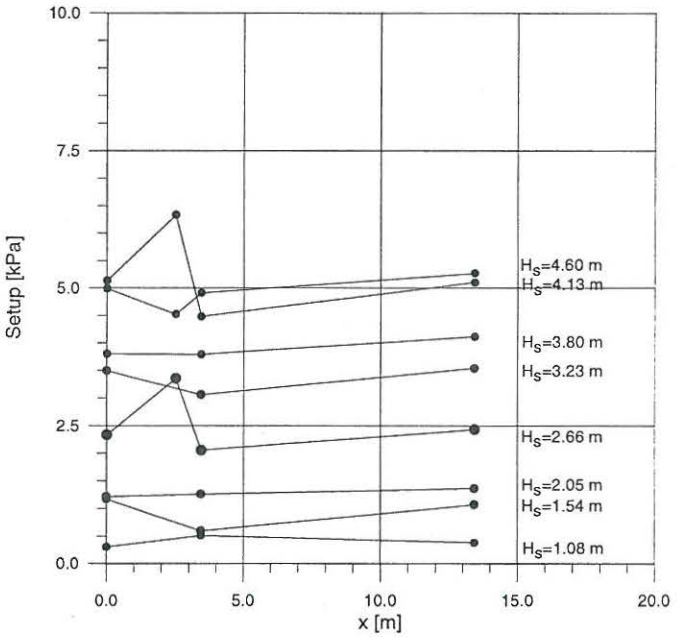

Figure 11: *Set-up in 1:65 model (distorted core 1:20) (Prototype units).*

It is seen from Figures 5-11 that the set-up is more or less constant through the core of the breakwater for a given wave condition. Only near the filter layer, the set-up seems to be slightly smaller than further inside the core. However, this is only seen for some of the tests. Because the breakwater is backfilled, it was expected that the set-up would increase with the distance from the outer face of the breakwater. This is only seen for the prototype.

II.C.1.3.2 Set-up as a function of incident wave height

In Figure 12, the set-up at the position of pressure transducer 27 is shown as a function of the incident wave height.

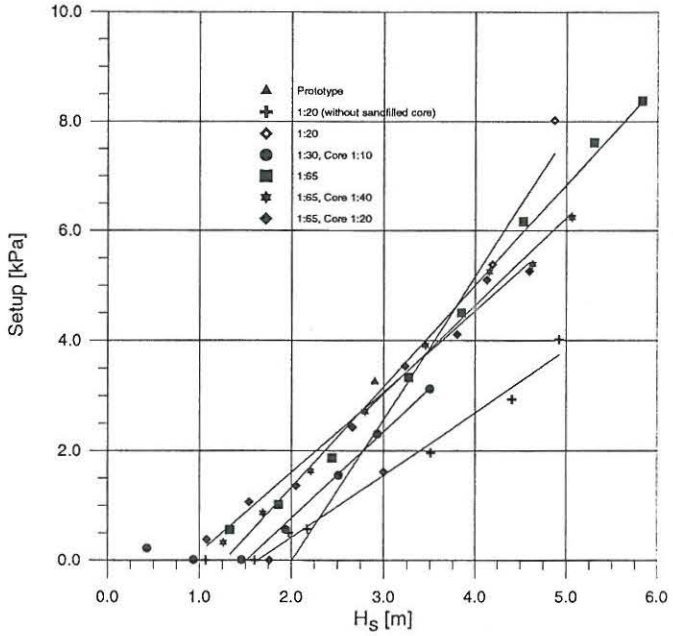

Figure 12: *Set-up (pressure transducer 27) as a function of the incident significant wave height.*

In general it is seen that there is relatively good similarity between the set-up in the prototype and the different scale models. Only the model in scale 1:20 without sandfilled core yields too small set-up, hence the porosity of this model is too large compared to the other models where the pores are filled with sand.

Furthermore, 12 shows that the set-up is linearly dependent on the incident wave height, and the wave height must exceed 1.0-2.0 m before any set-up is developed. The set-up varies between 0 for small wave heights and 15-20 % of the wave height for the largest wave heights, which corresponds very well to the rule of thumb by Bürger et al. (1988).

For the models at scale 1:65 with different core scaling the set-up is expected to be highest in the model with the finest core material. This is seen for the largest wave heights, but the differences in set-up for the three models are not very pronounced.

From these considerations it is seen that modelling the sandfill in the core is more important than modelling the grain size of the original core material.

II.C.1.4 Comparison between measured set-up and theoretical set-up

In Figure 13, the set-up determined by the theoretical expression presented in Sec-

tion II.C.1.2 is shown for five different periods. Furthermore, the measured set-up is indicated for the different tests. As described in Section II.C.1.2 several parameters are included in the theoretical formulation and the following parameters have been applied in Figure 13:

D=14 m
c=1.25 (Barends, 1988)
n=0.4
α=33.7°
K=1.0 m/s

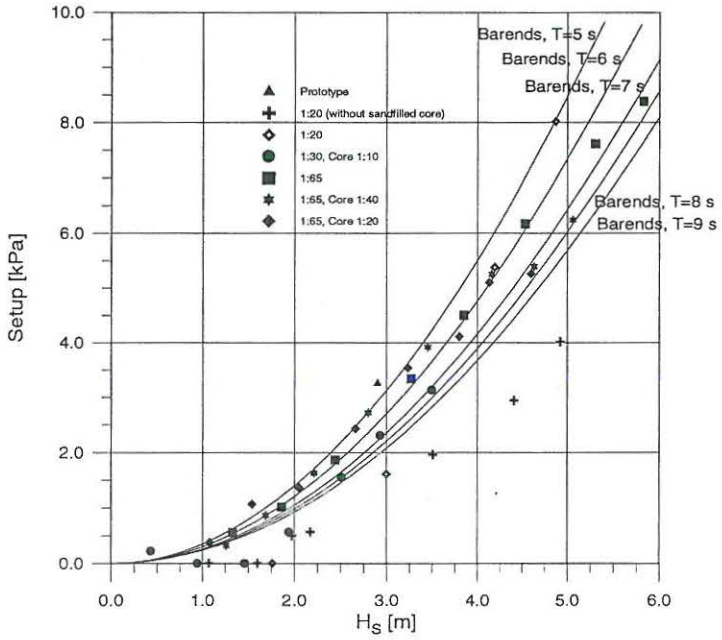

Figure 13: *Theoretical maximum average set-up and measured set-up at transducer 27.*

The theoretical set-up seems to correspond quite well to the measured set-up. However, the theoretical set-up is a power function of the wave height (for a given period), while the measured set-up increases linearly with increasing wave height as shown in Figure 12. This is due to the fact that a Pierson-Moskowitz spectrum has been applied. When the wave height increases, the period increases as well, and thus the set-up will increase because the wave height increases, but it will not increase that fast because the period increases as well. It is seen that also theoretically, the wave height must be of a certain magnitude before any significant set-up is developed

As mentioned above, several parameters have to be determined in order to apply the theoretical expression. The set-up is very sensitive to some of these parameters and e.g. the permeability and the air entrainment factor are very difficult to estimate.

Therefore it is possible to manipulate these parameters to fit the measured set-up, and thus the very good similarity between experimental and theoretical set-up as shown in Figure 13 should not be taken for more than it is.

II.D.2 Hydraulic gradients

In order to understand the complex phenomena occurring within the core of a breakwater, the hydraulic gradients are very important. In this section hydraulic gradients within the core of the Zeebrugge breakwater are presented for both model scale tests and prototype measurements. The gradients are determined for different incident wave heights and at different positions in the core. Only the tests with irregular waves with a water level of z=4.62 m have been applied. The first set of data from HRLB (without sandfilled core) have not been used in this analysis due to a different transducer location, which makes comparisons difficult. Due to time limits and missing transducers the second set of data from HRLB have not been applied either.

II.D.2.1 Determination of hydraulic gradients

The hydraulic gradients have been calculated using five sets of pressure cells each containing three cells, (PR10-PR19-PR26), (PR16-PR19-PR26), (PR12-PR10-PR19), (PR13-PR16-PR18), and (PR14-PR16-PR19). The positions of the cells are shown in Figure 14.

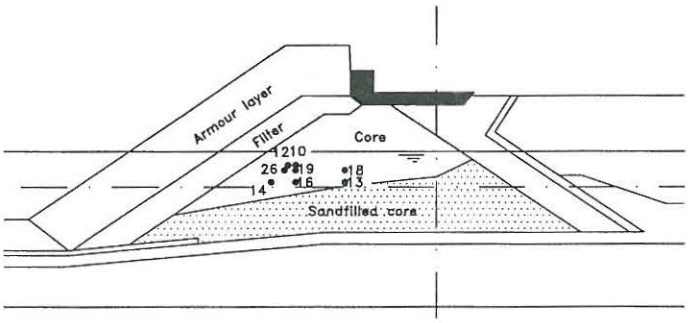

Figure 14: *Location of pressure cells.*

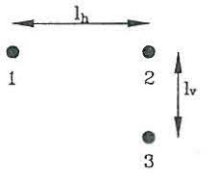

Figure 15: *Mutual location of pressure cells.*

According to the definition in Figure 15, the horizontal and vertical component of the resulting hydraulic gradient can be calculated as

$$i_{horiz}(t) = \frac{PR2(t) - PR1(t)}{l_h} \qquad i_{vert}(t) = \frac{PR2(t) - PR3(t)}{l_v} \tag{4}$$

whereas the resulting gradient and its direction are determined by

$$i_{res}(t) = \sqrt{i_{horiz}(t)^2 + i_{vert}(t)^2} \qquad \tan\Theta(t) = \frac{i_{vert}(t)}{i_{horiz}(t)} \tag{5}$$

II.D.2.2 Illustration of hydraulic gradients

Figures 16-20 show the plots of the five different hydraulic gradients for some of the tests. Only the gradients that are reliable are shown. For instance, the only gradient which is available from the model tests in scale 1:30 is (PR13-PR16-PR18). The plots are made by calculation of the resulting gradient and its direction for each timestep in each time series and subsequently averaging the results within every 10 degrees. A closed path is obtained from each of the sea states tested in the laboratory i.e., the plots obtained from AU-model tests each contain eight closed paths originating from the eight different tests with different wave heights (and periods). The model test data is scaled to prototype and axes are shown as [kPa/m]. The wave heights which yield the hydraulic gradients are shown in table 4.

1:65, core 1:65	1:65, core 1:40	1:65, core 1:20	1:30, core 1:10	Prototype
1.33 m	1.26 m	1.08 m	0.43 m	2.90 m
1.86 m	1.69 m	1.54 m	0.94 m	-
2.44 m	2.21 m	2.05 m	1.46 m	-
3.27 m	2.80 m	2.66 m	1.94 m	-
3.85 m	3.45 m	3.23 m	2.51 m	-
4.53 m	4.16 m	3.80 m	2.93 m	-
5.30 m	4.63 m	4.13 m	3.50 m	-
5.83 m	5.06 m	4.60 m	-	-

Table 4: *Wave height characteristics.*

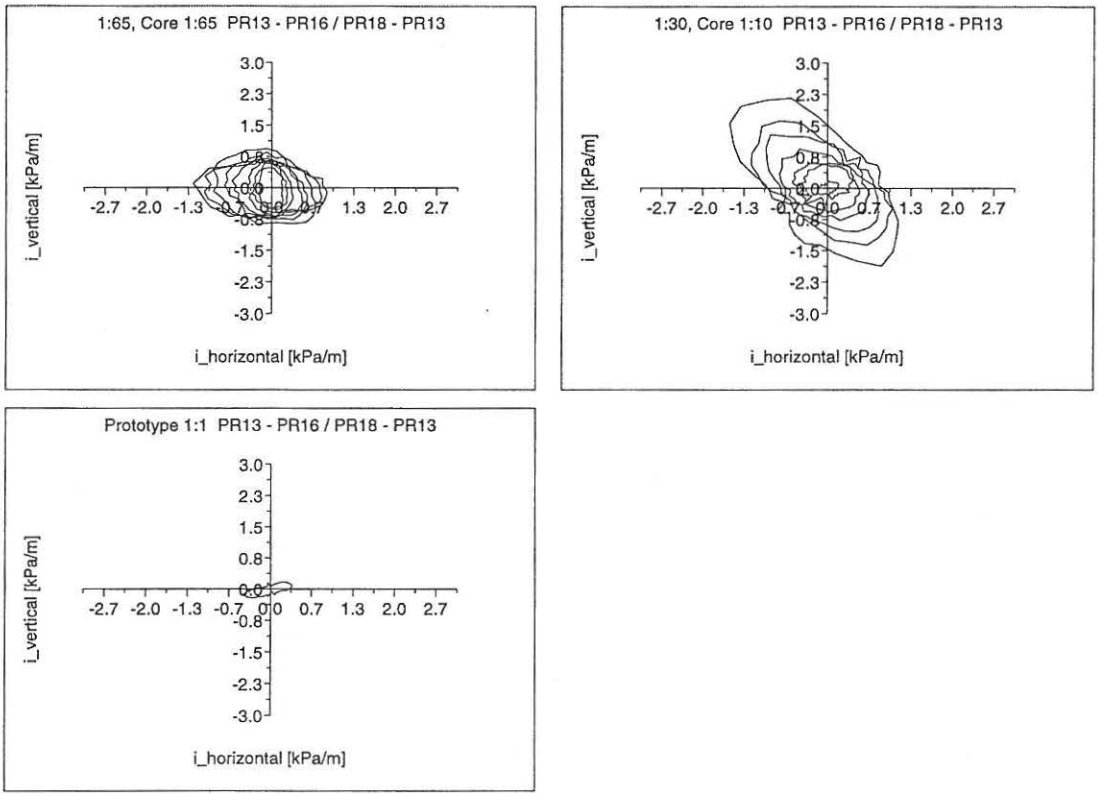

Figure 16: *Pressure gradients, PR13-PR16-PR18.*

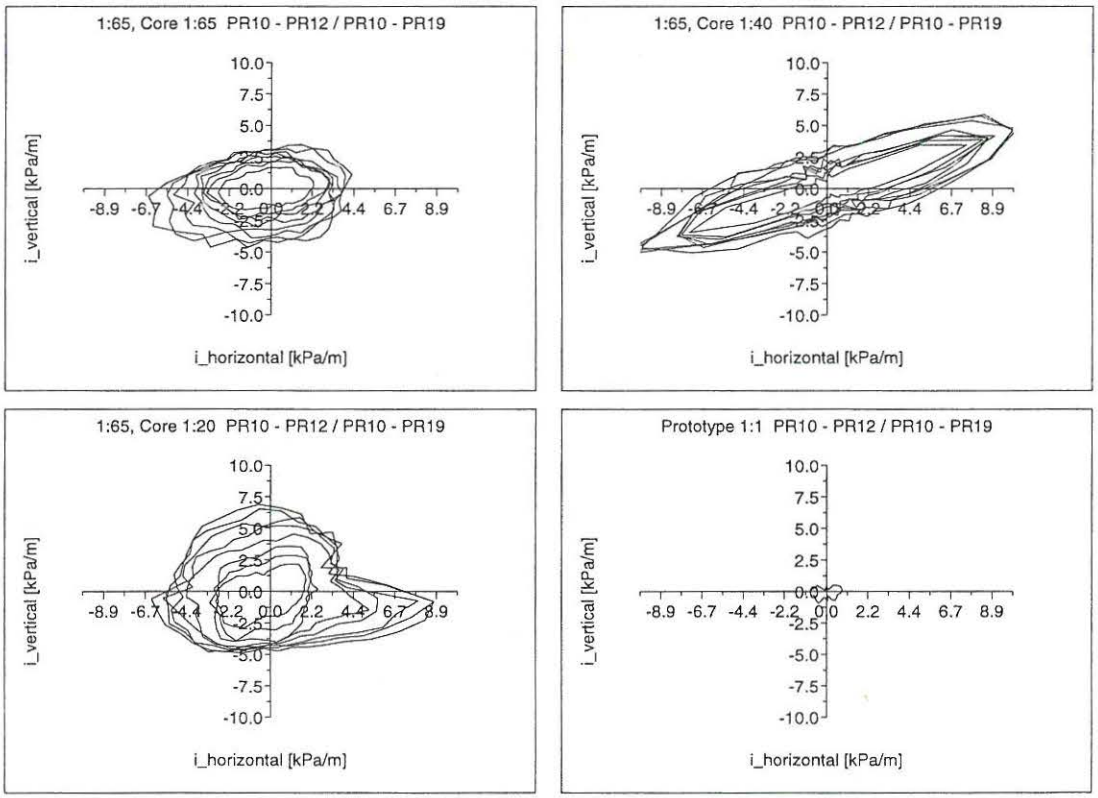

Figure 17: *Pressure gradients, PR10-PR12-PR19.*

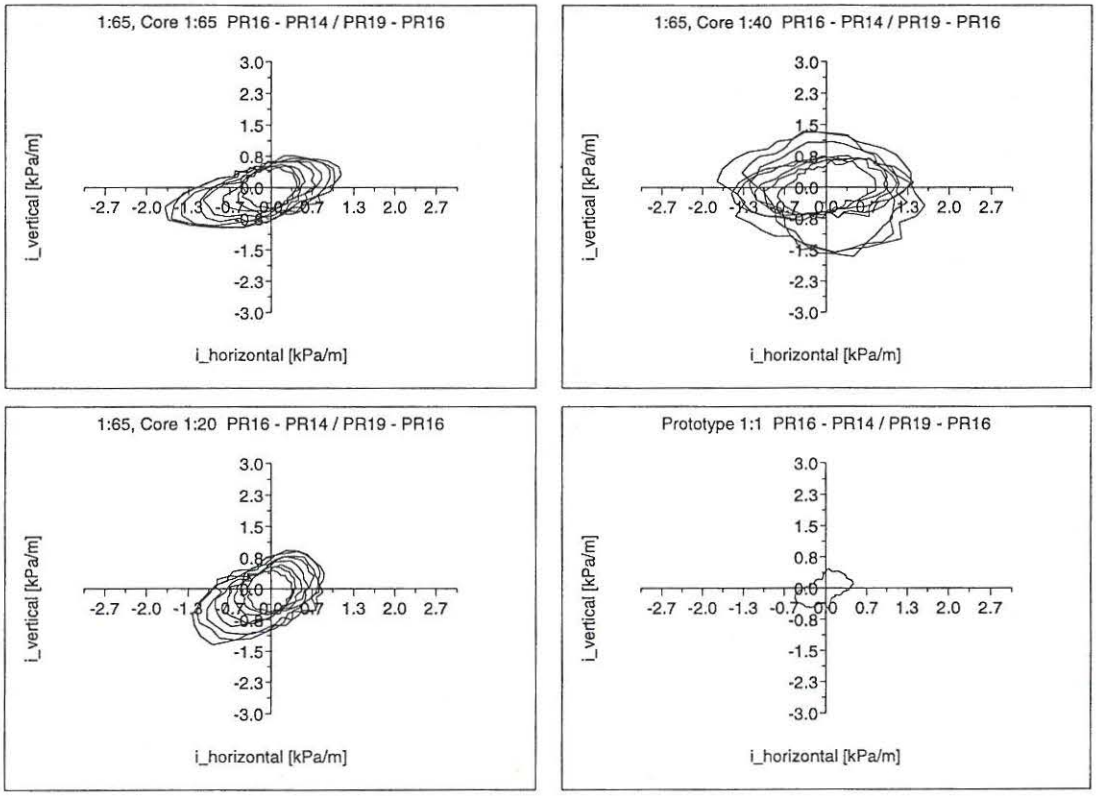

Figure 18: *Pressure gradients, PR14-PR16-PR19.*

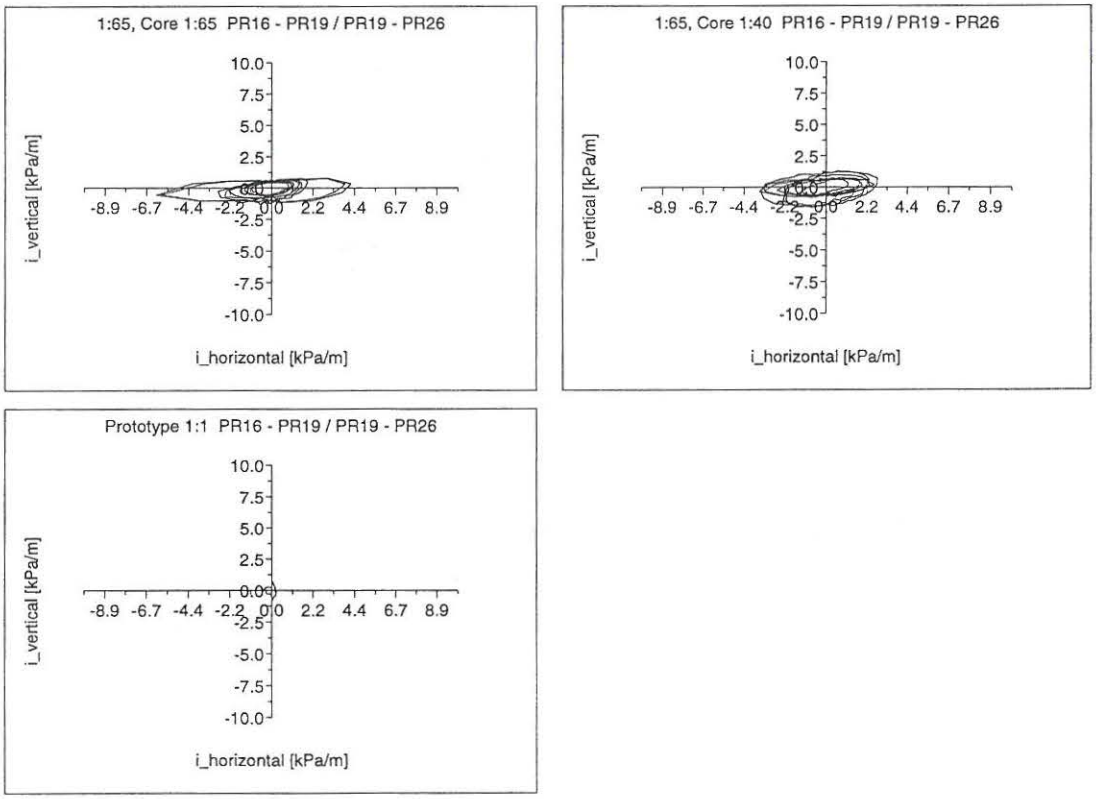

Figure 19: *Pressure gradients, PR16-PR19-PR26.*

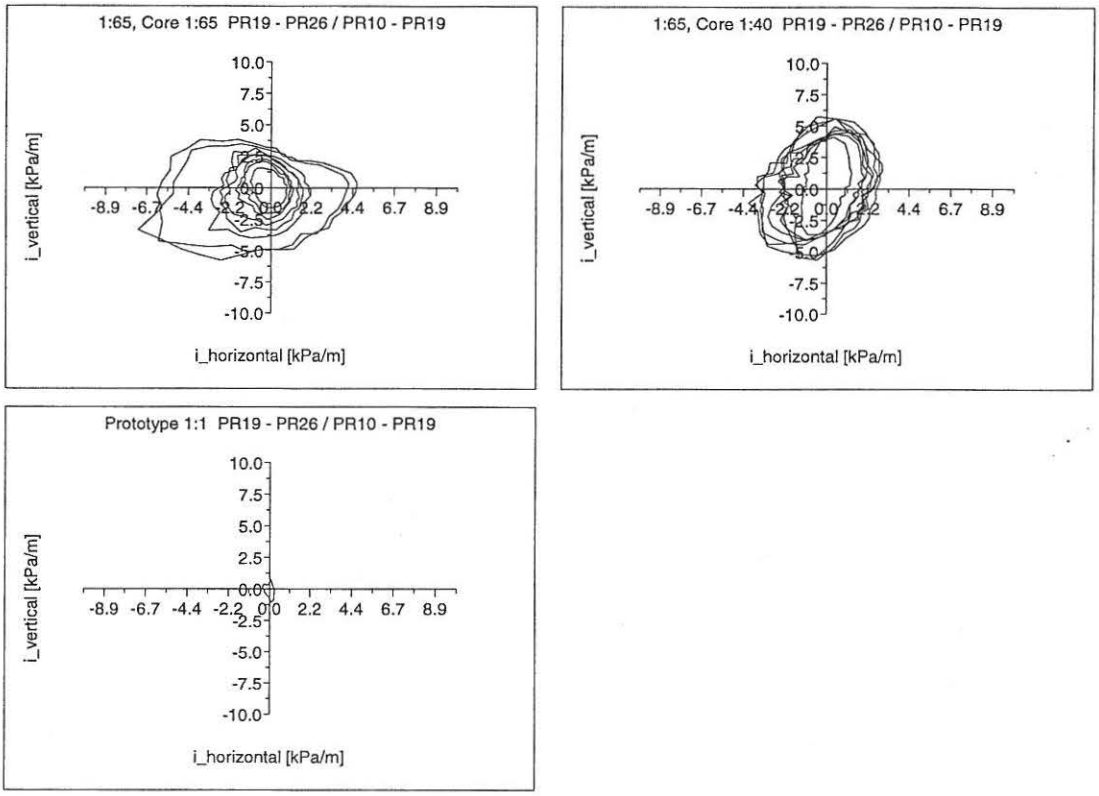

Figure 20: *Pressure gradients, PR10-PR19-PR26.*

The relevance of these kinds of plots is dependent of the placement of the pressure cells as well as the desired information to be extracted. If measurements were made within or just below the main armour layer, it could be of interest to investigate the relation between the size and direction of the prevailing gradients and the stability of the armour in terms of a critical gradient. In this case, though, the measurements are only made within the core of the breakwater and the plots can therefore only be interpreted by mutual comparisons and comparisons with phenomena related to the core such as internal setup and damping.

First of all, it is seen from Figures 16-20 that the hydraulic gradient increase for increasing wave height (the "diameter" of the closed paths increases, and the innermost curve of course correspond to the smallest wave height), and in most cases the shape of the path is independent of the wave height. However, the gradients seem to increase relatively rapidly for the two tests with the highest wave heights for the AU-model with strictly Froude scaling, and the flow becomes primarily horizontal (cf. Figures 16, 19, and 20).

If the plots from the model tests are compared with attaining plots from prototype a number of things can be observed. Regarding the scale 1:30, only the gradient (PR13-PR16-PR18) is available. From Figure 16 it is seen that the gradients from scale 1:30 are larger that the corresponding gradients from the 1:65 (core 1:65) model, and for high waves the main direction is also different.

In general, the magnitude of the gradients from the model tests are much larger than the the corresponding gradient in the prototype (please note that the gradients from the prototype are based on a wave height of 2.90 m). This leads to the conclusion that the models constitute more dense structures than expected (also for the models with distorted core material) or that the prototype may be more permeable than expected. Perhaps the sand infiltration is not as prounounced as expected. These observations agree with the fact that a linear scaling of the grain material size leads to a too dense structure in the smaller scale model where the Reynolds number is considerably smaller. However, the shape of the gradients are very similar in prototype and model tests.

It can also be concluded that the upper part of the instrumented area (comprising pressure cells PR10, PR12, PR19, and PR26) experience larger gradients than the lower part of the instrumented area i.e., the pressure fluctuations decrease with the vertical distance from the SWL. Particularly, the vertical component of the gradient decreases with the distance from SWL, see Figure 19.

It is seen that an assumption of no vertical and only horizontal hydraulic gradients i.e., a purely hydrostatic pressure distribution, which is implemented in a number of numerical models (including the FloX model) cannot be justified on the basis of the shown results. The plots show that the flow inside breakwaters must be considered as a complex flow in at least two dimensions.

As a final comment, it should be noted that especially the gradients determined from the three model tests in scale 1:65 are based on distances between the pressure sensors as small as 0.6 cm in model scale. The relative uncertainties on the distances between these sensors are therefore very large due to the monitoring uncertainty and this can highly influence on both the magnitude and direction of the hydraulic gradients.

II.D.3.2 Relation between β-value and Forchheimer's equation

Normally, when considering flow in porous media, the Forchheimer's equation or the extended Forchheimer equation is applied

$$i = au + bu|u| + c\frac{\partial u}{\partial t} \tag{6}$$

where i is the hydraulic gradient, u is the bulk velocity and a, b, and c are constants.

Because this relation is commonly used, it would be of interest to determine the theoretical relationship between the Forchheimer equation and the damping equation proposed by Oumeraci et al. (1990)

$$p(x) = p_0 e^{-\beta \frac{2\pi}{L'} x} \tag{7}$$

where p_0 is the pore pressure at x=0 and L' is the wave length within the breakwater. The derivation of Oumeraci et al. (1990) is based on a general linearized Bernoulli equation for an oscillatory flow in a wave filter

$$\frac{p}{\rho_w} + k_v \frac{\partial \varphi}{\partial t} + gz + c_f \varphi = const. \tag{8}$$

where

p : pressure
ρ_w: density of water
k_v: constant depending on porosity (n) and inertia effects (D): $k_v = \frac{D}{n}$
φ : velocity potential
g : acceleration of gravity
z : vertical coordinate
c_f: linearized friction coefficient

From this generalized Bernoulli equation and appropriate boundary conditions Oumeraci et al. (1990) derived the damping expression presented in equation (7)

Differentiating equation (8) with respect to x yield

$$\begin{aligned} \frac{\partial p}{\partial x} &= -\rho_w k_v \frac{\frac{\partial \varphi}{\partial x}}{\partial t} - \rho_w g \frac{\partial z}{\partial x} - \rho_w c_f \frac{\partial \varphi}{\partial x} \\ &= -\rho_w k_v \frac{\partial u}{\partial t} - \rho_w g \frac{\partial z}{\partial x} - \rho_w c_f u \end{aligned} \tag{9}$$

where u is the velocity. Equation (9) and the approximation of the hydraulic gradient $i \approx -\frac{1}{\rho_w g}\frac{\partial p}{\partial x}$ yield

$$i = \frac{k_v}{g}\frac{\partial u}{\partial t} + \frac{\partial z}{\partial x} + \frac{c_f}{g}u \tag{10}$$

This expression is almost similar to the Forchheimer equation. The first term is an acceleration term, the second term is a hydrostatic term, and the third term are the laminar term. Therefore the damping theory by Oumeraci et al. (1990) corresponds to the application of the form of the Forchheimer equation in (10).

However, the turbolent term (u^2) in equation (6) is normally predominant when considering internal flow in breakwaters, and this turbolent term does not occur in (10), hence there is no evident purpose in relating the β-value in equation (7) to the coefficients in the Forchheimer equation.

The above analysis may suggest that the model derived by Oumeraci et al. in equation 7 is too simple beeing a linear model compared with the non-linear Forchheimer model.

This paragraph has rendered the considerations made by AU up till now but should not be regarded as a concluded analysis. It could be of relevance to derive an extended version of equation 7 starting the derivation from the non-linear equation.

References

Barends, F.B.J., 1988: *Discussion on paper by Simm and Hedges:"Pore pressure response and stability of rubble mound breakwaters."* Breakwaters 1988.

Bürger, W., Oumeraci, H, Partenscky, H.W., 1988: *Geohydraulic investigations of rubble mound breakwaters.* In Proceedings of ICCE, 1988.

Oumeraci, H., Partenscky, H.W., 1990: *Wave-induced pore pressures in rubble mound breakwaters.* In Proceedings of ICCE, 1990.